IEEE Access
Multidisciplinary ⋮ Rapid Review ⋮ Open Access Journal

Received 28 July 2022, accepted 24 August 2022, date of publication 5 September 2022, date of current version 29 September 2022.

Digital Object Identifier 10.1109/ACCESS.2022.3204039

RESEARCH ARTICLE

A Hybrid Modeling Method for Aluminum Smelting Process Based on a Hybrid Strategy-Based Sparrow Search Algorithm

YASONG LUO, JIAYANG DAI, XINGYU CHEN, AND YILIN LIU

Guangxi Key Laboratory of Intelligent Control and Maintenance of Power Equipment, School of Electrical Engineering, Guangxi University, Nanning 530004, China

Corresponding author: Jiayang Dai (daijiayang@gxu.edu.cn)

ABSTRACT In the production of aluminum, the regenerative aluminum smelting process is an important part for energy efficiency and product quality. Aluminum liquid temperature is a significant variable in the aluminum smelting process, and it is costly to measure timely because it requires protective temperature sensor. To handle this problem, a kind of modeling framework which combine a mechanism model with multi-scale kernel technique is proposed. First, the mechanism model is built for the aluminum liquid temperature by the energy conservation law and heat transfer mechanism. Since the mechanism model is based on some assumptions, it often results in unknown variables. Thus, the multi-scale kernel technique is used to obtain the unknown variables. Finally, a hybrid temperature prediction model is built by combining the multi-scale kernel and the mechanism model. The parameter identification of the hybrid model is described as an optimization problem, and a hybrid strategy-based sparrow search algorithm (HSSA) is proposed to solve this problem. The experiment results show that HSSA has higher convergence accuracy and stronger global search ability than the original sparrow search algorithm (SSA), and the proposed hybrid model can correctly estimate the aluminum liquid temperature.

INDEX TERMS Regenerative aluminum smelting, mechanism modeling, multi-scale kernel, sparrow search algorithm.

I. INTRODUCTION

Aluminum has good ductility, plasticity, recyclability and oxidation resistance. Based on excellent physical and chemical properties, aluminum alloys are widely applied in automobile, aviation and military industries. The aluminum smelting process is an important part for the production of recycled aluminum. This process mainly smelts the scrap aluminum parts and aluminum smelting trimmings, and then recycled aluminum is produced through thermal insulation, casting and other processes. Besides, aluminum smelting can also be used for the remelting and reprocessing of various aluminum ingots. Aluminum smelting furnace is the key equipment for aluminum smelting and the main energy consuming equipment of the process. The traditional recuperative smelting technology has high fuel consumption, while the regenerative smelting technology has low energy consumption [1]. In the production of aluminum, the regenerative aluminum smelting process is an important part for energy efficiency and product quality. Aluminum liquid temperature is a significant variable in the aluminum smelting process, and it is costly to measure timely because it requires protective temperature sensor. Therefore, it is of practical significance to study the online prediction method of aluminum liquid temperature for monitoring the state of the aluminum smelting process.

Aluminum smelting is one of the typically complex industrial furnace production process. Many scholars have conducted a lot of related research on the modeling of complex

The associate editor coordinating the review of this manuscript and approving it for publication was Daniel Augusto Ribeiro Chaves.

This work is licensed under a Creative Commons Attribution-NonCommercial-NoDerivatives 4.0 License.
For more information, see https://creativecommons.org/licenses/by-nc-nd/4.0/

industrial furnaces. Gao *et al.* [2] modeled the pyrolysis and gasification processes of oil-bearing sludge to study the heat transfer characteristics of an industrial furnace. In this modeling, material equations of motion, heat transfer equations and kinetic equations were used to describe the pyrolysis process, while mass and energy equations were used to describe the gasification process. Alshehhi and Ali [3] presented a validated 3D Computational Fluid Dynamics (CFD) model to study the effects of burner position and orientation, chimney position and flow momentum on heat transfer of hot gas and furnace thermal efficiency, and the optimal design parameters were obtained. Li *et al.* [4] calculated the slag iron heat index by using the heat, carbon and oxygen balance in the high temperature zone of the blast furnace. Then, using the relationship between iron liquid temperature and slag iron heat index, the furnace temperature parameters are calculated when production conditions are changed. Zhou *et al.* [5] developed various CFD models to simulate complex multi-phase reactive flows in three regions of furnace, shaft, raceway and hearth for fault diagnosis and operational optimization of blast furnaces. Although the physical significance of this kind of mechanism modeling approach is relatively clear, for complex systems such as industrial furnaces, modeling often suffers from computational complexity and time consumption. Besides, certain assumptions or idealized modeling in order to study a particular problem leads to a reduction in the accuracy of the model. Hence, it is difficult to meet the requirements of experiment with only a single mechanism model.

Currently, more research on the modeling of industrial furnaces and similar processes is focused on data-driven approaches. In the aluminum smelting process, the collected data is highly non-linear and time-varying due to the fluctuating composition of the incoming material, the variety of metal impurities contained in aluminum and the complexity of the smelting process. For modeling strongly nonlinear processes such as industrial furnaces, Chen *et al.* [6] proposed a soft sensor modeling framework based on a double locally weighted kernel principal component regression with approximate linear correlation, and applied it to temperature prediction in a roller kiln furnace for lithium battery cathode materials. Chen *et al.* [7] considered more accurate predictions based on the paper [6] and constructed a data-driven error compensation model using real-time operational data. For the strongly non-linear, highly redundant and time-varying characteristics, an error compensation model was developed using a double locally weighted kernel principal component regression based on a dynamic window. Finally, the compensation model was combined with the mechanistic model to obtain a hybrid temperature prediction model. Wu *et al.* [8] proposed a stacked auto-encoder deep learning method based on just-in-time learning, and applied it to the modeling of industrial hydrocracking processes. Yang *et al.* [9] combined a mechanistic model of the smelting process with a data-driven approach using artificial intelligence technology. The uncertainty and error of the mechanism model were modeled by a neural network of unknown order. To effectively combine the mechanism model and the data-driven model, a new saturation alternation identification strategy was proposed. With the goal of obtaining accurate silicon content online to improve the quality of iron, a soft sensor method based on an adaptive stacked polymorphism model was proposed in the paper [10]. Considering the process time variability of blast furnace iron and silicon content prediction models, Li *et al.* [11] proposed a new data-driven modeling approach to ensure the accuracy of the model. First, a nonlinear T-S fuzzy model was constructed for the silicon content of iron liquid, and then the subsequent parameters of the fuzzy model were identified using a Bayesian approach to obtain probabilistic outputs. Saxén *et al.* [12] reviewed a data-driven time-discrete model for short-term time-discrete prediction of silicon content in blast furnace hot metal. Gultekin *et al.* [13] used a data-driven dynamic mode-following control decomposition method to model an inverter-fed induction motor. These papers above provided ideas for dealing with the time variability of aluminum smelting process. Qu *et al.* [14] proposed an artificial bee colony algorithm to optimize the classifier model of the kernel extreme learning machine. The introduction of the kernel method was beneficial to the classification and identification of power quality disturbance signals. Tang and Tian [15] could flexibly and stably process multi-source heterogeneous datasets through automatic adjustment of kernel parameters. In addition, using multiple kernels could enhance the interpretability of the model and improve the generalization performance of the classifier. Troncoso *et al.* [16] introduced a kernel function for time series data and used it for any data mining task that relies on similarity or distance measures. Bao *et al.* [17] established multi-scale kernels approach through a multi-kernel learning framework. This approach generalized well not only the dispersed regions of the training set but also the dense regions of the dataset. Huang *et al.* [18] extracted the main components of the neural network input by the kernel principal component analysis method and built a prediction model for furnace temperature by an improved extreme learning machine, obtaining better prediction capability and higher generalization capability. These papers provided the basic ideas for the research of this paper. Although this type of data-driven modeling approach enhanced the accuracy of model, it still had some disadvantages. Firstly, it required a large amount of data. Secondly, the distribution of data must include most of the situations in the actual factory, otherwise the data-driven model may not be applicable in some cases. Therefore, it is necessary to further study the mechanism and data in the process modeling to describe the aluminum smelting process more accurately.

Parameter identification is an important process in modern industrial process modeling. By properly optimizing and adjusting model parameters, it can guide the operation of the production process as much as possible. The problem of parameter identification usually can be described as an optimization problem. In recent decades, the swarm intelligence

optimization algorithm has become the main technology to solve the global optimization problem due to its simplicity, flexibility and efficiency. To date, many algorithms such as the firefly algorithm [19], the bat algorithm [20], the gray wolf algorithm [21], the ant lion algorithm [22], the whale algorithm [23], the salp swarm algorithm [24] and sparrow search algorithm (SSA) have been successively proposed by scholars. Among them, the sparrow algorithm (SSA) is a new swarm intelligence algorithm developed by Xue and Shen [25] based on the foraging and anti-predatory behavior of sparrows. SSA is capable of satisfying the global exploration and local exploitation abilities required by an optimization algorithm, hence it is widely applied in the identification of parameters in complex models. Yan and Song [26] used SSA to optimize Back-propagation (BP) neural network and applied it to coal mine water source data processing. Yuan and Zhao [27] proposed a distributed maximum power point tracking method based on improved sparrow search algorithm. Tuerxun and Chang [28] used the SSA for optimizing the penalty factor and kernel function parameters of support vector machines, and constructed a sparrow search algorithm-support vector machine wind turbine fault diagnosis model. Nevertheless, there are still problems such as slow convergence, weak global search ability, and the tendency to fall into local optimality when solving the optimization problem. In order to improve the performance of the SSA, Liu and Ye [29] used the Levy flight strategy to simulate the bat search predation behavior, thus essentially improving the optimization performance of the algorithm and reducing the algorithm parameters. Simulation tests with standard functions showed that the bat algorithm with Levy flight characteristics effectively improved the individual bat search ability, and convergence performance and search accuracy were significantly improved. Furthermore, Ma and Lu [30] combined SSA with improved tent chaos mutation, Levy flight mutation, learning mutation based on elite opposition, and variable radius mutation inter-combination to obtain SSA variants of the optimal algorithm. Lee and Kim [31] proposed a hybrid algorithm of parallel simulated annealing, which learns the Bayesian network structure through a greedy algorithm. Specifically, simulated annealing was then parallelized with memory to speed up the search process. In each step of local search, a hybrid search method combining simulated annealing and greedy algorithm improved the convergence accuracy. Elgamal *et al.* [32] introduced the chaotic initialization and simulated annealing mechanism into the Harris Eagle algorithm, which was compared with the grasshopper optimization algorithm, particle swarm optimization, genetic algorithm, butterfly optimization algorithm and ant lion algorithm one by one. A comparison of six learning algorithms through a neuron model was made by Gao *et al.* [33], including particle swarm optimization, genetic algorithm, ant colony optimization, evolutionary strategy and population-based incremental learning. In order to obtain larger data volume, better data utilization and higher proxy accuracy, Li *et al.* [34] proposed a new evolutionary algorithm framework. For the problem of complex material grinding factors and difficulty in accurately predicting yield particle size, Zhang *et al.* [35] introduced a chaotic initialization population to promote the global search ability. At the same time, the Cauchy mutation strategy was introduced to solve the local optimal problem, effectively improving the algorithm's search ability. Together, swarm intelligence methods have been improved by the above scholars extremely. However, in the face of complex industrial processes, swarm intelligence algorithms still suffer from unsatisfactory global search ability and a tendency to fall into local optimum. Therefore, it is necessary to further explore the application of swarm intelligence algorithm in combination with the characteristics of industrial furnaces. SSA is a new meta-heuristic algorithm with fewer control parameters and superior local search capability. Compared with other algorithms, the introduction of some strategies such as the simulated annealing mechanism and weighting factors, allows the SSA to avoid falling into local optima while ensuring convergence. Subsequent experimental simulations also show that the hybrid strategy-based sparrow algorithm outperforms other algorithms in terms of convergence and convergence speed, and is more suitable for handling similar non-linear optimization problems in industrial furnaces.

In summary, many scholars have proposed a great variety of methods on the modeling and parameter optimization of industrial furnaces and complex industrial processes. However, due to the complex thermodynamics of the aluminum smelting process and the large fluctuation of incoming materials, these approaches are difficult to be directly applied to aluminum smelting process. Therefore, this paper designs a process hybrid modeling approach that combines process mechanics and data to predict aluminum liquid temperature. Besides, a hybrid strategy-based sparrow search algorithm (HSSA) is proposed to identify the parameters of the model. The subsequent subsections of this paper are structured as follows. Section 2 analyzes the problems existing in the aluminum smelting process. In the third section, a hybrid modeling approach for aluminum smelting process is proposed. The fourth section describes the parameter identification problem of the hybrid model, and proposes an improved sparrow optimization algorithm. Section 5 verifies the effects of the proposed model and algorithm through experiments. Section 6 is the conclusion.

II. ANALYSIS OF PROBLEMS IN ALUMINUM SMELTING PROCESS

As shown in the flow chart of recycled aluminum smelting (Fig. 1), the smelting is the critical process and aluminum smelting furnace is the main equipment in aluminum recycle. The structure of regenerative aluminum smelting furnace is shown in Fig. 2, consisting of a furnace chamber, a regenerative burner (containing a burner and a regenerative pool), a reversing device and a smoke exhaust device. The two burners are not in the same working condition during normal operation of the regenerative burner. When one of the burners

is in the combustion operation, its fuel channel is open, and cold air through the incandescent heat accumulator is heated to hot air for fuel combustion. At the same time, another burner in the heat storage state, its fuel channel is closed, and the combustion products enter into the heat accumulator under the action of the fan through the combustion channel. Hence, the heat accumulates in the heat accumulator and is discharged through the smoke exhaust device. From the analysis of aluminum smelting production process and field experience, the temperature of aluminum liquid is a key variable in the aluminum smelting process. In actual production, the temperature of aluminum liquid needs to be measured by a thermocouple with a protective jacket, and the life of the thermocouple is short, which increases the production cost.

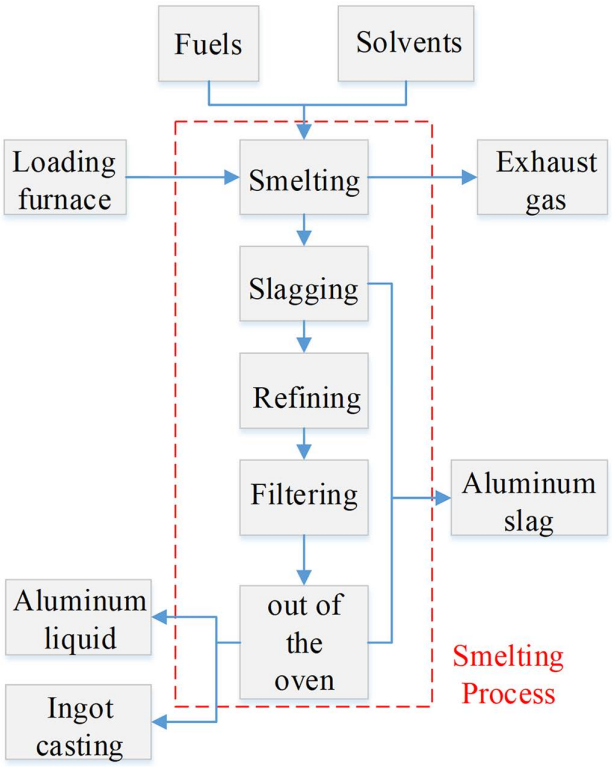

FIGURE 1. Flow chart of recycled aluminum smelting.

To handle the problems in the aluminum smelting process, this paper proposes a hybrid modeling method that combine a mechanism model with multi-scale kernels to predict the aluminum liquid temperature. Firstly, through heat transfer analysis and energy conservation principle, the mechanism model between aluminum liquid temperature and input variables is established. In this mechanism model, there are some variables that cannot be measured. Multi-scale kernel technology is introduced to estimate these unknown variables. Then, HSSA is proposed to optimize the model parameters. Finally, the accuracy and efficiency of the proposed approach are verified by actual industrial data.

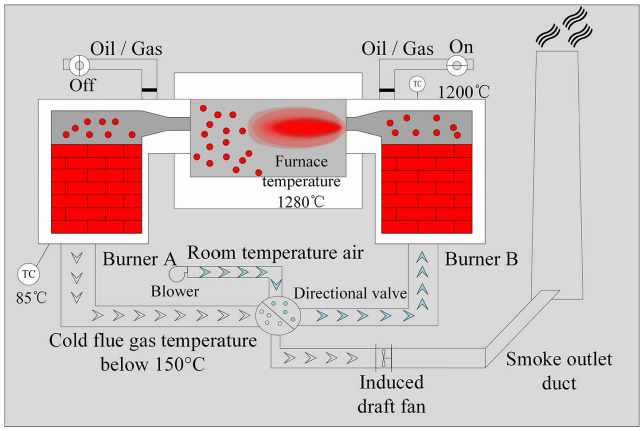

FIGURE 2. Working structure diagram of regenerative smelting furnace.

III. HYBRID MODELING OF THE ALUMINUM SMELTING PROCESS

A. MODELING OF ALUMINUM LIQUID TEMPERATURE BASED ON HEAT TRANSFER MECHANISM

Through heat transfer mechanism, the relationship between temperature change and heat change is established. Firstly, the furnace is considered as a heat balance system, and the heat income and heat outcome in the smelting furnace are analyzed. As shown in Fig. 3. Q1, Q2, Q3, Q4, and Q5 are heat income, and Q6, Q7, Q8, Q9, and Q10 are heat outcome.

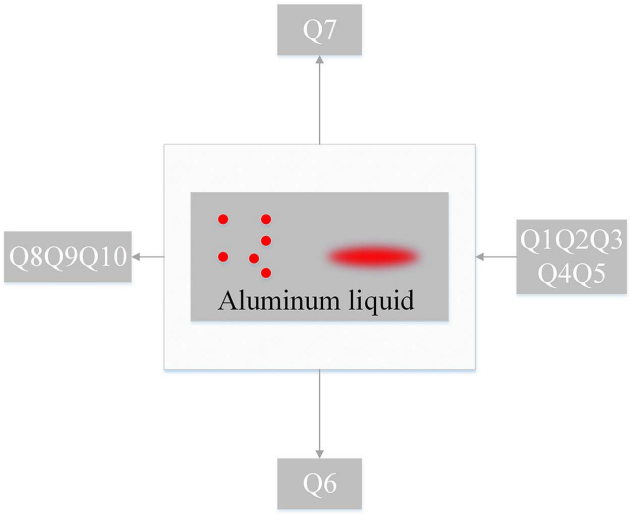

FIGURE 3. Energy change in aluminum smelting process.

According to the energy conservation law and heat transfer mechanism, the relational equation of Q1-Q10 is established. The specific equations are shown in Table 1, and some of the variables involved are shown in Table 2. The following assumptions are made: the temperature of the material entering the furnace, the temperature of air before enters the furnace, the gas temperature, and the temperature of the ambient air are regarded as the temperature of the material entering the furnace. The assumptions can be represented as

$T_{rl}(t) = T_k(t) = T_r(t) = T_f(t)$. C_s represents the average specific heat capacity (J/kg· °C) corresponding to each heat, and m_s represents the corresponding mass (kg) of each heat, where $s \in [1, 10]$.

As shown in Fig. 3, Q1 is the heat brought in by the material, Q2 is the heat brought in by the air, Q3 is the heat brought in by the natural gas, Q4 is the heat generated by the combustion reaction, and Q5 is the heat generated by the burning loss of the aluminum liquid. Heat outcome items: Q6 is the heat of material smelting, Q7 is the heat dissipation of the furnace body, Q8 is the heat taken away by the flue gas, Q9 is the heat taken away by the slag, and Q10 is the heat dissipation of the furnace.

TABLE 1. Heat calculation table.

Symbol	Calculation	Symbol	Calculation
Q1	$Q_1 = C_{rl} m_{rl} T_{rl}(t)$	Q6	$Q_{cl,1} = C_{cl,s} m_{cl} (T_m(t) - T_{rl}(t))$ $Q_{cl,2} = m_{cl} L$ $Q_{cl,3} = C_{cl,l} m_{cl} (T_{cl}(t) - T_m(t))$
Q2	$Q_2 = C_k m_k T_k(t)$	Q7	$Q_7 = 3.6 K_i (T_o(t) - T_f(t)) A_i \tau$
Q3	$Q_3 = C_r m_r T_r(t)$	Q8	$Q_8 = C_y m_y T_y(t)$
Q4	$Q_4 = m_r Q_{dw}$	Q9	$Q_9 = C_z m_z T_z(t)$
Q5	$Q_5 = M_{rl} \alpha Q_{yl}$	Q10	$Q_{10} = K_i'(\hat{T}(t) - T_o(t))$

According to the heat income and heat outcome in the smelting furnace, equation (1) is used to establish the differential equation of aluminum liquid temperature:

$$\frac{dT}{dt} = h(Q_{income} - Q_{outcome}) \tag{1}$$

TABLE 2. Variable comparison.

Symbol	Instruction	Symbol	Instruction
ϕ_1	Combustion air flow	T_z	Slag temperature
ϕ_2	Gas flow	T_y	Flue gas temperature
ϕ_3	Air-fuel ratio	T_o	Outer wall temperature
$\hat{T}$	Furnace chamber temperature	T_m	Material smelting temperature
T_{rl}	Temperature of material into the furnace	T_{cl}	Material discharge temperature

Combined with Table 1 and equation (1), the dynamic model of aluminum liquid temperature is got by some mathematical operations, and it is established as

$$f(t) = \frac{d\hat{T}(t)}{dt} = h_1 T_{rl}(t) + h_2 T_m(t) + h_3 T_{cl}(t) + h_4 T_y(t) + h_5 T_z(t) + h_6 T_o(t) + h_7 \hat{T}(t) + h_8 \tag{2}$$

where $h_1, h_2, h_3, h_4, h_5, h_6, h_7, h_8$ are the influence coefficients. In this model, the smelting temperature of material T_m, the temperature of the materials entering the furnace T_{rl} and the temperature of flue gas T_y can be obtained from the industrial data. With regard to the material discharge temperature T_{cl}, slag temperature T_z and outer wall temperature T_o, it is difficult to measure online and they are related to various factors such as combustion air flow, gas flow, air-fuel ratio and so on. At the same time, it is difficult to obtain the three temperatures through mechanism analysis. Therefore, we use the data of combustion air flow, gas flow, air-fuel ratio and other data to estimate T_{cl}, T_z and T_o in the mechanism model through the kernel function method.

B. UNMEASURED TEMPERATURE ESTIMATION METHOD BASED ON MULTI-SCALE KERNEL

The material discharge temperature, slag temperature, and outer wall temperature are difficult to measure online and are related to many factors. The functional relationship of these three temperatures cannot be directly measured or obtained through data calculation, and the unknown functional relationship in the mechanism model can be constructed by the kernel function. While it is difficult for a single kernel function to handle the data with different temporal characteristics. Hence, a multi-scale kernel method is proposed to deal with this problem. The Gaussian kernel function is used to build a multi-scale kernel function. Then, the unknown functional relationship in the mechanism model is constructed through the Gaussian kernel function. Taking the slag temperature as an example, a function is constructed to estimate the slag temperature, described as follows:

$$\hat{T}_z(t) = Q(\varphi(t)) \tag{3}$$

The slag temperature is related to the combustion air flow rate φ_1, the gas flow rate φ_2, and the air-fuel ratio φ_3, so the function $\varphi(t)$ can be described as:

$$\varphi(t) = [\varphi_1(t), \varphi_2(t), \varphi_3(t)]^T \tag{4}$$

The kernel functions with different scales are fused together to obtain the function Q. The increments of φ_1, φ_2 and φ_3 are used as the variables of the kernel function, represented as

$$K_z(\varphi(t), \varphi(t-1)) = \exp(-\frac{\|\varphi(t) - \varphi(t-1)\|^2}{2\delta^2}) \tag{5}$$

where δ is the bandwidth of the kernel function. By using m different δ, we can obtain multi-scale Gaussian kernel functions:

$$\exp(-\frac{\|\varphi(t) - \varphi(t-1)\|^2}{2\delta_1^2}), \ldots \exp(-\frac{\|\varphi(t) - \varphi(t-1)\|^2}{2\delta_m^2}), \tag{6}$$

where $\delta_1 < \ldots < \delta_m$. When the bandwidth δ is small, the kernel function becomes steeper and is suitable for samples with large variation. Conversely, kernel function with larger bandwidth is suitable for samples that vary less. Through the

combination of multiple scale kernel functions, the model can achieve good performance for data with different trends, thus getting better generalization ability. To improve the efficiency of multi-scale kernel learning, the method of weighted summation kernel is adopted. Assume that K is a multi-scale kernel function, which is obtained by synthesizing m basic kernel functions of different scales.

$$K = \varepsilon_1 K_1 + \varepsilon_2 K_2 + \ldots + \varepsilon_m K_m, \quad \sum_{j=1}^{m} \varepsilon_j = 1, \quad \varepsilon_j \geq 0 \tag{7}$$

where ε_j is the weighting coefficient of the kernel function K_j.

$$K_j = \exp(-\frac{\|\varphi(t) - \varphi(t-1)\|^2}{2\delta_j^2}), \quad j = 1, 2, \ldots m, \quad \delta_1 < \delta_2 < \cdots < \delta_m \tag{8}$$

By using the multi-scale kernel to estimate T_{cl}, T_z and T_o, the hybrid model can be obtained as follows

$$f(t) = \frac{dT(t)}{dt} = h_1 T_{rl}(t) + h_2 T_m(t) + h_3 K_{cl} + h_4 T_y(t) + h_5 K_Z + h_6 K_o + h_7 T(t) + h_8 \tag{9}$$

$$K_{cl} = \sum_{j=1}^{m} \varepsilon_{clj} K_j \tag{10}$$

$$K_Z = \sum_{j=1}^{m} \varepsilon_{zj} K_j \tag{11}$$

$$K_o = \sum_{j=1}^{m} \varepsilon_{oj} K_j \tag{12}$$

The parameter identification of model (9) is described as an optimization problem:

$$\begin{aligned} &\min_{\theta} \ J(\theta) = \sqrt{\sum_{i=1}^{N} (T_i - \hat{T}_i(\theta))^2} \\ &s.t \quad \theta \in \left(\mathrm{P}_{\min}, \mathrm{P}_{\max}\right) \\ &\qquad \frac{d\hat{T}_i(\theta)}{dt} = f(t) \end{aligned} \tag{13}$$

where $\hat{T}_i$ is the predicted temperature of the aluminum liquid, T_i is the temperature of actual aluminum liquid, N is the number of samples. θ is the parameter to be identified in the model, and can be described as $\theta = [\varepsilon_{z1}, \varepsilon_{z2}, \ldots \varepsilon_{zm}, \varepsilon_{cl1}, \varepsilon_{cl2}, \ldots \varepsilon_{clm}, \varepsilon_{o1}, \varepsilon_{o2}, \ldots \varepsilon_{om}, \delta_1, \delta_2, \ldots \delta_m, h_1 \ldots h_8]$. P_{min} and P_{max} are the upper and lower bounds of θ.

Since the optimization problem contains a nonlinear model as an equation constraint, the traditional gradient-based method is difficult to find the global optimal solution. The sparrow algorithm has the advantages of high solution accuracy, fast convergence, and good stability in dealing with the optimization-seeking problem, However, it still has the problems of low accuracy, slow speed, and easy to be trapped in local optimum when facing the multi-peaked problem. Hence, based on the sparrow optimization algorithm, an improved sparrow optimization algorithm is proposed to solve the above problems.

IV. BATTERY TEST SYSTEM AND MODEL PARAMETER IDENTIFICATION

SSA is mainly inspired by the foraging behavior and anti-predation behavior of sparrows. Individuals in SSA are divided into three types: discoverers, followers and sparrows who are aware of the danger. The identity of discoverers and followers is dynamic and changing. The discoverer provides the foraging area and direction for the population, the follower follows the discoverer to forage, and the sparrow who is aware of the danger is responsible for the surveillance around. During the foraging process, the positions of three types of individuals will be continuously updated to obtain the optimal food source, and the position of the optimal food source is the found optimal solution [25]. In this paper, we improve SSA in terms of improving the initialization position, updating the position iterations, and avoiding local convergence as follows.

A. IMPROVING CHAOS FACTOR INITIALIZATION POPULATIONS

The sparrow algorithm starts by randomly initializing the sparrow population and defining the relevant parameters, as well as defining the maximum number of iterations. The initialized population is.

$$X^0 = \begin{bmatrix} x_{1,1} & x_{1,2} & \cdots & x_{1,d} \\ x_{2,1} & x_{2,2} & \cdots & x_{2,d} \\ \vdots & \vdots & \vdots & \vdots \\ x_{n,1} & x_{n,2} & \cdots & x_{n,d} \end{bmatrix} \tag{14}$$

where n is the number of sparrows, d shows the dimension of the variables to be optimized. The improvement is done by introducing a chaos factor to update the initialized population,

$$X_{i,j}^{v+1} = \sin(\frac{b\pi}{X_{i,j}^{v}}) \tag{15}$$

where v indicates the current iteration, $b \in (0, 1)$, $X_{i,j}^{v}$ represents the value of the jth dimension of the ith sparrow at the vth iteration. The search space is made to have better uniformity and increase the population diversity. The fitness of the initial population is then calculated and ranked to select the current best and worst values.

B. IMPROVEMENT OF NON-INERTIAL WEIGHTING FACTOR STRATEGY

The location update strategy of the discoverer is described as follows.

$$X_{i,j}^{v+1} = \begin{cases} X_{i,j}^{v} \exp\left(-\dfrac{i}{\alpha \times iter_{\max}}\right) & if \ R_2 < ST \\ X_{i,j}^{v} + Q \times L & if \ R_2 \geq ST \end{cases} \tag{16}$$

where v indicates the current iteration, $j = 1, 2, \ldots, d$. $iter_{max}$ is the maximum number of iterations, which takes the value of 1000. $i \in (0, 100)$, $\alpha \in (0, 1)$ are a random number. R_2 ($R_2 \in (0, 1)$) and ST ($ST \in [0.5, 1]$) represent the alarm value and the safety threshold, respectively. Q is a random number that follows a normal distribution. L shows a $1 \times$ d of the matrix, where each element inside is 1. When $R_2 < ST$, it means that there are no predators around and the finder goes into wide search mode. If $R_2 \geq ST$, it means that some sparrows found the predator and all sparrows need to fly quickly to other safe areas. By introducing a nonlinear inertia weighting factor.

$$w(v) = 0.01 \times \left(2^{\frac{iter_{\max} - v}{iter_{\max}}} - 1\right)$$

$$X_{i,j}^{v+1} = \begin{cases} X_{i,j}^{v} \exp\left(-\dfrac{i}{\alpha \times iter_{\max}}\right) \times w(v) & if\ R_2 < ST \\ \left(X_{i,j}^{v} + Q \times L\right) \times w(v) & if\ R_2 \geq ST \end{cases} \tag{17}$$

where v is the number of the current iterations, 0.01 is the weighting factor. $X_{i,j}^{v}$ denotes the value of the jth dimension of the ith sparrow at the v iteration. The weights will decrease nonlinearly as the number of iterations increases. Larger nonlinear weights in the early iterations are good for global search, and smaller nonlinear weights in the later iterations are good for local search.

C. IMPROVEMENT OF LEVY FLIGHT STRATEGY

The location update strategy of the follower is described as follows

$$X_{i,j}^{v+1} = \begin{cases} Q \exp\left(\dfrac{X_{worst} - X_{i,j}^{v}}{i^2}\right) & if\ i > \dfrac{n}{2} \\ X_{p}^{v+1} + Q \times L & otherwise \end{cases} \tag{18}$$

where X_p is the optimal position occupied by the finder. X_{worst} denotes the current global worst location. A indicates a $1 \times d$ of the matrix for which each element inside is randomly assigned to 1 or -1, $A^{+} = A^{T}(AA^{T})^{-1}$. When $i >$ n/2, it represents that the ith follower with the worse fitness value is not getting food and is in a very hungry state, Hence, it needs to fly to other places to forage for more energy. When $i \leq$ n/2, the sparrow moves around the optimal location.

Add Levy flight strategy when $i \leq$ n/2.

$$Levy(d) = 0.01 \times \frac{r_1 \times \lambda}{|r_2|^{\left(\frac{1}{\rho}\right)}}$$

$$\lambda = \left(\frac{\Gamma(1+\rho) \times \sin\frac{\pi\rho}{2}}{\Gamma(\frac{1+\rho}{2}) \times \rho \times 2^{\left(\frac{(\rho-1)}{2}\right)}}\right)^{\left(\frac{1}{\rho}\right)} \tag{19}$$

where d denotes the dimension of the variables to be optimized. ρ is a constant. r_1, r_2 are random numbers in the range [0,1]. Gamma function on the set of real numbers for positive integers is x, where $\Gamma(x) = (x-1)!$. In the process of finding the optimal solution, Levy flight strategy can not only perform local search in short distance but also global search in long distance. Therefore, when searching near the optimal value, Levy can enhance the local search ability and effectively solve the problem of standard sparrow algorithm falling into local optimum.

Then update the location of the sparrow who is aware of the danger, the location update strategy is described as follows.

$$X_{i,j}^{v+1} = \begin{cases} X_{best}^{v} + \beta \left|X_{i,j}^{v} - X_{best}^{v}\right| & if\ f_i > f_g \\ X_{i,j}^{v} + \hat{K}\left(\dfrac{\left|X_{i,j}^{v} - X_{\text{worst}}^{v}\right|}{(f_i - f_w) + \varepsilon}\right) & if\ f_i = f_g \end{cases} \tag{20}$$

where X_{best}^{v} is the current global optimal position. β, as the step control parameter, is a normal distribution of random numbers with a mean value of 0 and a variance of 1. $\hat{K} \in [-1, 1]$ is a random number. f_i is the current fitness value of the sparrow. f_g and f_w are the best and worst fitness values calculated for the current global, respectively. ε is the smallest constant to avoid zero-division-error. For simplicity, when $f_i > f_g$ indicates that the sparrow is at the edge of the group. X_{best} represents the location of the sparrow center, the surrounding area is safe. The farther $X_{i,j}^{v}$ is from X_{best}, the more the position needs to move. $f_i = f_g$ shows that the sparrows in the middle of the population are aware of the danger and need to get close to others. $\hat{K}$ is the direction in which the sparrow moves and is also the step control factor coefficient.

D. INTRODUCTION OF SIMULATED ANNEALING MECHANISM

To prevent the sparrow algorithm from falling into local optimum, a simulated annealing mechanism is introduced. That is, when the fitness value of the next iteration position is greater than the fitness value of the current global optimum position, there is still a certain probability of accepting an inferior solution. The annealing temperature $\tilde{T}$ determines the probability of receiving an inferior solution for the sparrow population, and $\tilde{T}$ decreases with the number of iterations. The expression of $\tilde{T}$ is

$$\tilde{T}(v+1) = \hat{\alpha}\tilde{T}(v) \tag{21}$$

where v denotes the number of iterations, $\hat{\alpha}$ denotes the annealing coefficient and takes the value of [0.9, 1]. Comparing the new position F_{v+1} adaptation with the original adaptation F_v.

$$\Delta F = F_{v+1} - F_v \tag{22}$$

When $\Delta F \leq 0$, accept the new position. When $\Delta F > 0$, judging from the following formula,

$$\exp\left(\frac{-\Delta F}{\tilde{T}}\right) \geq rand(0, 1) \tag{23}$$

If the equation (23) holds, the new position is accepted, and vice versa, the new position is not accepted.

Table 3 is the pseudocode form of HSSA.

E. TIME COMPLEXITY ANALYSIS OF HSSA

The time complexity of SSA [25] is $t = O(d+\hat{f}(d))$, d shows the dimension of the variables to be optimized. n is the number of sparrows. $\hat{f}(d)$ denotes the objective function solving time. The time of HSSA population initialization parameters is ψ_1. The chaotic mapping time of each dimension is ψ_2. The initialization time is $t_1 = O(\psi_1 + n(\hat{f}(d) + \psi_2 d))$. The time to update the producer location to generate a random number is ψ_3. The time for each dimension position update of the producer is ψ_4. The generation time of adaptive coefficients is ψ_5. The total time of the producer location update is $t_2 = O(n(\psi_3 + \psi_4 + \psi_5)d))$. The time to update the follower location to generate a random number is ψ_6, The time for each dimension position update of the follower is ψ_7. The time to introduce the Levy flight coefficient is ψ_8. The total time of the follower location update is $t_3 = O(n(\psi_6 + \psi_7 + \psi_8)d))$. The time to update the location of the aware of the dangerous sparrow has not changed, for t_4. In the simulated annealing mechanism, the time to generate random numbers is ψ_9. The time for the annealing temperature update is ψ_{10}. The total time spent by the simulated annealing mechanism is $t_5 = O(\psi_9 + \psi_{10})$. The total time complexity of HSSA is $t' = t_1 + iter_{\max}(t_2 + t_3 + t_4 + t_5) = O(d + \hat{f}(d)) = t$. Because HSSA has the same time complexity as SSA, it does not improve performance by sacrificing extra time.

V. SIMULATION EXPERIMENTS

A. HSSA PERFORMANCE COMPARISON AND ANALYSIS

In this section, to test the hybrid model, it is applied to an industrial regenerative smelting furnace. 1000 samples are collected from November 1 to 3, 2017, of which 800 samples are used as training samples, and 200 samples are used as testing samples. MAX, MSE, the root mean squared error (RMSE), the mean absolute error (MAE), and the decision coefficient (R2), are used as the performance indices, which are shown in Equations (24)-(28).

$$MAX = \max(Y - y) \tag{24}$$

$$MSE = \frac{1}{\hat{N}} \sum_{i=1}^{\hat{N}} (Y - y)^2 \tag{25}$$

$$RMSE = \sqrt{\frac{1}{\hat{N}} \sum_{i=1}^{\hat{N}} (Y - y)^2} \tag{26}$$

$$MAE = \frac{1}{\hat{N}} \sum_{i=1}^{\hat{N}} |Y - y| \tag{27}$$

$$R^2 = 1 - \frac{MSE(Y, y)}{Var(y)} \tag{28}$$

where $\hat{N}$ is the number of samples, Y is the predicted value of the aluminum liquid temperature. y is the actual value of the aluminum liquid temperature. $Var(y)$ is the variance of y.

1) ANALYSIS ON SIMULATION OF DIFFERENT IMPROVEMENT STRATEGIES FOR HSSA

First, analyze different improvement strategy on algorithm performance. The sparrow algorithm with a single improvement strategy refers to the introduction of only one of the chaos factor, weight factor, Levy flight strategy and simulated annealing mechanism. The predictions of the hybrid model optimized by the four improved strategy on the 200 testing samples are tested 50 times for each strategy. The four methods are denoted as CSSA (chaos factor), NSSA (weighting factor), LSSA (Levy flight) and SSSA (simulated annealing mechanism). In the parameter identification of the hybrid model, the dimension of the variables is set to 36, the number of sparrows is set to 100, and the max iterations is set to 1000. It can be seen from the Table 4 that the prediction results of the four methods are significantly improved compared with the original algorithm.

2) COMPARISON OF DIFFERENT KINDS OF INTELLIGENT OPTIMIZATION ALGORITHMS

To further show the performance of HSSA, the original SSA [25], the grey wolf algorithm (GWO) [21] and the sine cosine algorithm (SCA) [36] are used to optimize the hybrid model. The performance comparison on the testing samples is shown in Table 5. It can be seen from the Table 5, HSSA outperforms the original SSA, GWO, and SCA in each performance index. The detailed predictions are given in Fig. 4 and Fig. 5. From the two figures, the results show that the hybrid model optimized by HSSA has better compensation results than SSA, GWO, and SCA in predicting the aluminum liquid temperature.

The convergence curves of each algorithm are given in Fig. 6. The results show that SSA and HSSA converge faster than the GWO and SCA algorithms. It can be seen from the first 100 convergence curves that HSSA is slightly slower than the original SSA due to the introduction of the simulated annealing algorithm to accept the local optimal solution. However, the previous results show that in terms of time complexity, the improvement of HSSA performance does not come at the expense of time. And HSSA has better prediction accuracy.

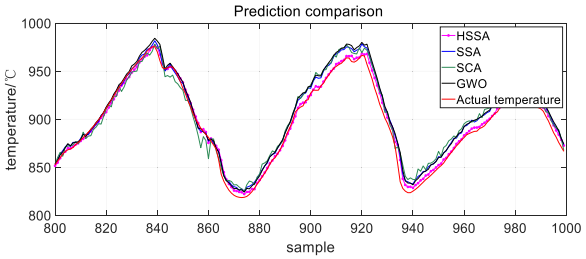

FIGURE 4. Comparison of different algorithms for temperature prediction.

B. MODEL VERIFICATION

To evaluate the performance of the proposed hybrid modeling method, the number m of multi-scale kernels should

TABLE 3. Pseudocode form of HSSA.

Algorithm 1 The framework of the HSSA

Input: G: the maximum iteration

PD: the number of the producers

SD: the number of the sparrows who perceive the danger

R2: the alarm value Establish an objective function $f(X)$, where variable $X_i(i = 1, 2, ..., d)$.

Initialize a population of n sparrows and define its relevant parameters.

Output: X_{best}(Optimal solution) and f_g(Fitness value)

while the maximum iterations G is not met **do**
  Rank the fitness values and find the current best
  $R2 = rand(1)$
  for $i = 1 : PD$ **do**
    Update the sparrow location by Eq.(17)
  end for
  for $i = (PD + 1) : n$ **do**
    Update the sparrow location by Eq.(19)
  end for
  for $i = 1 : SD$ **do**
    Update the sparrow location by Eq.(20)
  end for
  Get the current new location;
  If the new location is better than before, update it;
  $t = t+1$;
end while
return X_{best}, f_g

TABLE 4. Results of different improvement strategies.

Method	MAX	MSE	RMSE	MAE	R2
SSA	27.6745	62.6521	7.9153	6.1486	0.9850
CSSA	24.6907	48.9808	6.9986	5.5263	0.9883
NSSA	25.7401	45.4734	6.7434	5.2772	0.9891
LSSA	25.1301	43.5980	6.6029	5.1700	0.9896
SSSA	22.9969	37.3792	6.1139	4.8390	0.9911

TABLE 5. Comparison of the results of different algorithms.

Algorithms	MAX	MSE	RMSE	MAE	R2	TIME
SSA	26.4596	62.7795	7.9233	6.2083	0.9850	146.641
HSSA	15.6921	28.1627	5.3069	4.2225	0.9933	143.229
GWO	30.4156	56.0971	7.4898	5.8705	0.9866	123.918
SCA	29.8919	32.1015	6.4150	4.7381	0.9901	120.763

be determined first. By changing the number m, Table 6 shows the prediction accuracy of the hybrid model on testing samples. From Table 6, m is set as a proper value of 7. After the number of multi-scale kernels is determined, the parameters in the model need to be identified as a whole in order to obtain the optimal performance. The parameters to be identified include the weight coefficients of the multi-scale kernel ε_j, the bandwidth δ_j and the impact coefficients h. Let the vector of parameters to be identified as $\theta = [\varepsilon_{z1}, \varepsilon_{z2}, \ldots \varepsilon_{zm}, \varepsilon_{cl1}, \varepsilon_{cl2}, \ldots \varepsilon_{clm}, \varepsilon_{o1}, \varepsilon_{o2}, \ldots \varepsilon_{om}, \delta_1, \delta_2, \ldots \delta_m, h_1, \ldots h_8]$. The number of sparrows is set to $N = 100$. The proportion of discoverers and followers of the sparrow algorithm is set as 20%. The alarm threshold ST is chosen to be 0.8. The upper and lower limits are set as $[-100,100]$, and the dimension of the variables is set as 36. The search ranges of the kernel function width parameter δ_j and the weight parameter ε_j are set as $[-10,10]$ and $[-50,50]$, respectively. By applying HSSA algorithm, the optimal parameter combination is obtained, the results are shown in the Table 7.

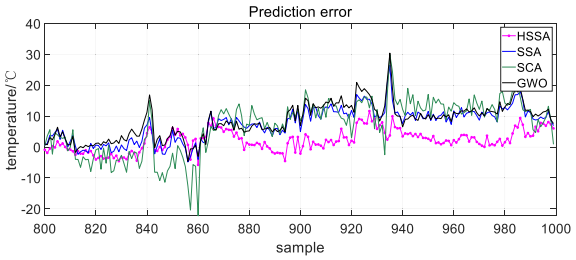

FIGURE 5. Comparison of prediction errors of different algorithms.

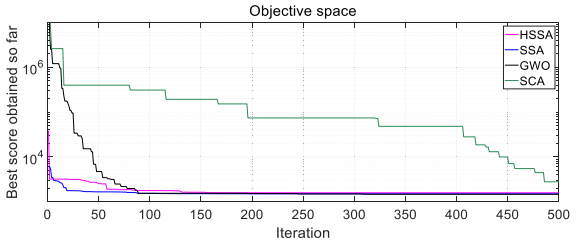

FIGURE 6. Convergence curve of different algorithms.

TABLE 6. Experiments on the number of multi-scale kernel functions1.

m	MAX	MSE	RMSE	MAE	R2
3	24.2451	35.3373	5.9445	4.7567	0.9915
4	23.2024	43.7053	6.6110	5.2595	0.9895
5	27.1500	58.6747	7.6599	6.1130	0.9860
6	25.3631	31.8081	5.6399	4.4796	0.9924
7	23.4543	30.9526	5.5635	4.3409	0.9926
8	27.8122	66.8492	8.1761	6.7202	0.9840
9	27.4094	58.6719	7.6598	6.1459	0.9860
10	27.8951	60.5372	7.7806	6.0371	0.9855

For performance comparison, the initial mechanism model is used to predict the aluminum liquid temperature. The three temperatures that cannot be directly measured in the initial mechanism model are treated as parameters. After optimized by HSSA, the compared results between the initial mechanism model and the hybrid model are shown in the Table 8. The detailed prediction results are showed as Fig. 7 and Fig. 8.

TABLE 7. Results of optimal parameter combination.

Parameters	Solutions	Parameters	Solutions	Parameters	Solutions
ε_{z1}	0.6998	ε_{cl6}	0.8925	δ_4	0.6871
ε_{z2}	16.5927	ε_{cl7}	0.8597	δ_5	0.8961
ε_{z3}	0.8474	ε_{o1}	2.3681	δ_6	0.1229
ε_{z4}	2.3689	ε_{o2}	6.5071	δ_7	0.9118
ε_{z5}	0.7658	ε_{o3}	-2.9006	h_1	1.1581
ε_{z6}	0.8857	ε_{o4}	1.1679	h_2	0.0108
ε_{z7}	-26.4831	ε_{o5}	1.5981	h_3	0.3687
ε_{cl1}	0.8908	ε_{o6}	1.0251	h_4	-0.1931
ε_{cl2}	0.5828	ε_{o7}	-19.0671	h_5	0.7991
ε_{cl3}	1.2881	δ_1	0.8204	h_6	-37.1861
ε_{cl4}	3.0199	δ_2	0.4393	h_7	1.2541
ε_{cl5}	0.7298	δ_3	0.3814	h_8	0.1684

In Fig. 7 and Fig. 8, the red line is the predicted temperature and the black line is the actual temperature.

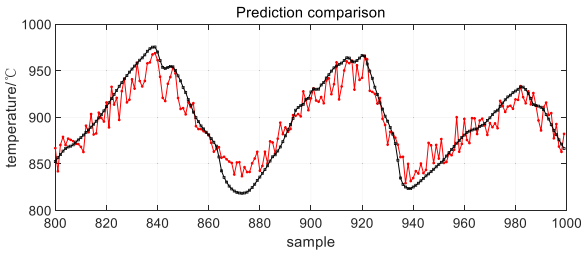

FIGURE 7. Temperature prediction results of the initial model.

TABLE 8. Comparison of prediction results on different models.

Model	MAX	MSE	RMSE	MAE	R2
Initial mechanism model	87.2465	453.1490	21.2873	16.5612	0.8915
Hybrid model	22.4941	30.3056	5.5051	4.3558	0.9927

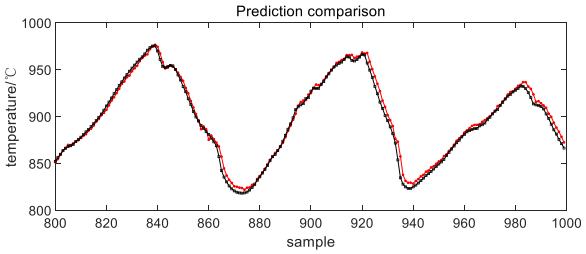

FIGURE 8. Temperature prediction results of the hybrid model.

It can be seen from Fig. 7 and Fig. 8, the prediction curves of the hybrid model are closer to the actual curves. From Table 8, the five performance indices of the hybrid model are better than the initial mechanism model. The results show that the proposed hybrid modeling has a better performance for the prediction of the aluminum liquid temperature.

VI. CONCLUSION

To handle the problem of aluminum liquid temperature prediction in smelting furnaces, a prediction modeling methods that combine a mechanism model with multi-scale kernels is proposed. In this modeling framework, due to the high nonlinearity of the input and output variables of the aluminum smelting process, the initial mechanism model of the process is established by the energy conservation law and heat transfer mechanism. For the three temperatures in the mechanism model that are difficult to measure online, a multi-scale kernel method is proposed to deal with this problem, and the hybrid model is obtained. In addition, the problem of parameter identification for the hybrid model is described as an optimization problem. A hybrid strategy-based sparrow search algorithm is designed to solve the optimization problem, effectively improving the model performance. The simulation experiments results show the effectiveness of the proposed method.

REFERENCES

[1] F. Wang and B. Gu, "Energy-saving technology and development of aluminum smelting furnace," in *Proc. Chongqing Foundry Annu. Conf.*, 2019, pp. 290–293.
[2] N. Gao, X. Jia, and G. Gao, "Modeling and simulation of coupled pyrolysis and gasification of oily sludge in a rotary kiln," *Fuel*, vol. 279, Nov. 2020, Art. no. 118152.
[3] S. Alshehhi and M. Ali, "Reverberatory furnace CFD modeling for efficient design: Burners and chimney location," in *Proc. Int. Mech. Eng. Congr. Expo.*, Pittsburgh, PA, USA, 2018, Art. no. V06AT08A022.
[4] Z. Li, M. Chu, and Z. Liu, "Furnace heat prediction and control model and its application to large blast furnace," *High Temp. Mater. Processes*, vol. 38, no. 2019, pp. 884–891, 2019.
[5] C. Zhou, G. Tang, and J. Wang, "Comprehensive numerical modeling of the blast furnace ironmaking process," *JOM*, vol. 68, no. 5, pp. 1353–1362, 2016.
[6] N. Chen, J. Dai, X. Yuan, W. Gui, W. Ren, and H. N. Koivo, "Temperature prediction model for roller kiln by ALD-based double locally weighted kernel principal component regression," *IEEE Trans. Instrum. Meas.*, vol. 67, no. 8, pp. 2001–2010, Aug. 2018.
[7] N. Chen, J. Dai, and X. Yuan, "Temperature prediction for roller kiln based on hybrid first-principle model and data-driven MW-DLWKPCR model," *ISA Trans.*, vol. 98, pp. 403–417, Mar. 2020.
[8] Y. Wu, D. Liu, X. Yuan, and Y. Wang, "A just-in-time fine-tuning framework for deep learning of SAE in adaptive data-driven modeling of time-varying industrial processes," *IEEE Sensors J.*, vol. 21, no. 3, pp. 3497–3505, Feb. 2021.
[9] J. Yang, T. Chai, C. Luo, and W. Yu, "Intelligent demand forecasting of smelting process using data-driven and mechanism model," *IEEE Trans. Ind. Electron.*, vol. 66, no. 12, pp. 9745–9755, Dec. 2019.
[10] Y. Fang, Z. Jiang, D. Pan, W. Gui, and Z. Chen, "Soft sensors based on adaptive stacked polymorphic model for silicon content prediction in ironmaking process," *IEEE Trans. Instrum. Meas.*, vol. 70, pp. 1–12, 2021.
[11] J. Li, C. Hua, Y. Yang, and X. Guan, "Data-driven Bayesian-based Takagi–Sugeno fuzzy modeling for dynamic prediction of hot metal silicon content in blast furnace," *IEEE Trans. Syst., Man, Cybern., Syst.*, vol. 52, no. 2, pp. 1087–1099, Feb. 2022.
[12] H. Saxen, C. Gao, and Z. Gao, "Data-driven time discrete models for dynamic prediction of the hot metal silicon content in the blast furnace—A review," *IEEE Trans. Ind. Informat.*, vol. 9, no. 4, pp. 2213–2225, Nov. 2013.
[13] M. A. Gultekin, Z. Zhang, and A. Bazzi, "Data-driven modeling of inverter-fed induction motor drives using DMDc for faulty conditions," in *Proc. IEEE Int. Electr. Mach. Drives Conf. (IEMDC)*, May 2021, pp. 1–5.
[14] L.-P. Qu, C.-L. He, J. Zhang, and T.-L. Gao, "Recognition of power quality disturbance based on artificial bee colony algorithm to optimize kernel extreme learning machine," in *Proc. 20th Int. Symp. Distrib. Comput. Appl. Bus. Eng. Sci. (DCABES)*, Dec. 2021, pp. 131–135.

[15] J. Tang and Y. Tian, "A multi-kernel framework with nonparallel support vector machine," *Neurocomputing*, vol. 266, pp. 226–238, Nov. 2017.
[16] A. Troncoso, M. Arias, and J. C. Riquelme, "A multi-scale smoothing kernel for measuring time-series similarity," *Neurocomputing*, vol. 167, pp. 8–17, Nov. 2015.
[17] J. Bao, Y. Chen, L. Yu, and C. Chen, "A multi-scale kernel learning method and its application in image classification," *Neurocomputing*, vol. 257, pp. 16–23, Sep. 2017.
[18] Q. Huang, S. Lei, C. Jiang, and C. Xu, "Furnace temperature prediction of aluminum smelting furnace based on KPCA-ELM," in *Proc. Chin. Autom. Congr. (CAC)*, Nov. 2018, pp. 1454–1459.
[19] X. S. Yang, *Nature-Inspired Metaheuristic Algorithms*. London, U.K.: Luniver Press, 2008.
[20] X. Yang and X. He, "Bat algorithm: Literature review and applications," *Int. J. Bio-Inspir. Com.*, vol. 5, pp. 141–149, Aug. 2013.
[21] S. Mirjalili, S. M. Mirjalili, and A. Lewis, "Grey wolf optimizer," *Adv. Eng. Softw.*, vol. 69, pp. 46–61, Mar. 2014.
[22] S. Mirjalili, "The ant lion optimizer," *Adv. Eng. Softw.*, vol. 83, pp. 80–98, May 2015.
[23] S. Mirjalili and A. Lewis, "The whale optimization algorithm," *Adv. Eng. Softw.*, vol. 95, pp. 51–67, Feb. 2016.
[24] S. Mirjalili, A. H. Gandomi, S. Z. Mirjalili, S. Saremi, H. Faris, and S. M. Mirjalili, "Salp swarm algorithm: A bio-inspired optimizer for engineering design problems," *Adv. Eng. Softw.*, vol. 114, pp. 163–191, Dec. 2017.
[25] J. Xue and B. Shen, "A novel swarm intelligence optimization approach: Sparrow search algorithm," *Syst. Sci. Control Eng.*, vol. 8, no. 1, pp. 22–34, Jan. 2020.
[26] P. Yan, S. Shang, C. Zhang, N. Yin, X. Zhang, G. Yang, Z. Zhang, and Q. Sun, "Research on the processing of coal mine water source data by optimizing BP neural network algorithm with sparrow search algorithm," *IEEE Access*, vol. 9, pp. 108718–108730, 2021.
[27] J. Yuan, Z. Zhao, Y. Liu, B. He, L. Wang, B. Xie, and Y. Gao, "DMPPT control of photovoltaic microgrid based on improved sparrow search algorithm," *IEEE Access*, vol. 9, pp. 16623–16629, 2021.
[28] W. Tuerxun, X. Chang, G. Hongyu, J. Zhijie, and Z. Huajian, "Fault diagnosis of wind turbines based on a support vector machine optimized by the sparrow search algorithm," *IEEE Access*, vol. 9, pp. 69307–69315, 2021.
[29] C. Liu and C. Ye, "Algorithm with the characteristics of Levy flights," *CAAI Trans. Intell. Syst.*, vol. 8, no. 3, pp. 240–246, 2013.
[30] B. Ma, P. Lu, L. Zhang, Y. Liu, Q. Zhou, Y. Chen, Q. Qi, and Y. Hu, "Enhanced sparrow search algorithm with mutation strategy for global optimization," *IEEE Access*, vol. 9, pp. 159218–159261, 2021.
[31] S. Lee and S. B. Kim, "Parallel simulated annealing with a greedy algorithm for Bayesian network structure learning," *IEEE Trans. Knowl. Data Eng.*, vol. 32, no. 6, pp. 1157–1166, Jun. 2020.
[32] Z. M. Elgamal, N. B. M. Yasin, M. Tubishat, M. Alswaitti, and S. Mirjalili, "An improved Harris Hawks optimization algorithm with simulated annealing for feature selection in the medical field," *IEEE Access*, vol. 8, pp. 186638–186652, 2020.
[33] S. Gao, M. Zhou, Y. Wang, J. Cheng, H. Yachi, and J. Wang, "Dendritic neuron model with effective learning algorithms for classification, approximation, and prediction," *IEEE Trans. Neural Netw. Learn. Syst.*, vol. 30, no. 2, pp. 601–614, Feb. 2019.
[34] J.-Y. Li, Z.-H. Zhan, H. Wang, and J. Zhang, "Data-driven evolutionary algorithm with perturbation-based ensemble surrogates," *IEEE Trans. Cybern.*, vol. 51, no. 8, pp. 3925–3937, Aug. 2021.
[35] S. Zhang, J. Zhang, Z. Wang, and Q. Li, "Regression prediction of material grinding particle size based on improved sparrow search algorithm to optimize BP neural network," in *Proc. 2nd Int. Symp. Comput. Eng. Intell. Commun. (ISCEIC)*, Aug. 2021, pp. 216–219.
[36] S. Mirjalili, "SCA: A sine cosine algorithm for solving optimization problems," *Knowl.-Based Syst.*, vol. 96, pp. 120–133, Mar. 2016.

YASONG LUO received the B.S. degree in electrical engineering and automation from the Chengdu University of Information Technology, in 2019. He is currently pursuing the M.S. degree majored in energy power (electrical engineering) with the School of Electrical Engineering, Guangxi University. His research interests include soft sensors, intelligent algorithms, modeling, and optimization of complex systems.

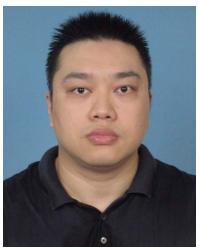

JIAYANG DAI received the B.S., M.S., and Ph.D. degrees from Central South University, in 2009, 2012, and 2019, respectively. He is currently an Assistant Professor with the School of Electrical Engineering, Guangxi University. His research interests include soft sensor, machine learning, reinforcement learning and optimization, and control of complex systems.

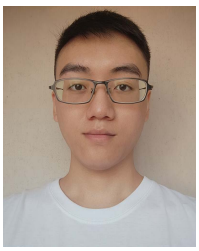

XINGYU CHEN received the B.S. degree in mechanical design manufacturing and automation from Xidian University, in 2020. He is currently pursuing the M.S. degree majored in control engineering with the School of Electrical Engineering, Guangxi University. His research interests include soft sensor, modeling, and optimization of complex systems.

YILIN LIU received the B.S. degree in automation from Guangxi University, in 2020, where he is currently pursuing the M.S. degree majored in control engineering with the School of Electrical Engineering. His research interests include soft sensor, intelligent algorithm, optimization, and control of complex systems.